PERGAMON

International Journal of Solids and Structures 40 (2003) 1995–2016

INTERNATIONAL JOURNAL OF SOLIDS and STRUCTURES

www.elsevier.com/locate/ijsolstr

Predictions of bifurcation and instabilities during dynamic extension

S. Mercier, A. Molinari *

Laboratoire de Physique et Mécanique des Matériaux, UMR CNRS 7554, ISGMP, Université de Metz, Ile du Saulcy, 57045 Metz Cedex, France

Received 17 February 2002; received in revised form 19 November 2002

Abstract

Dynamic bifurcation and flow instabilities of cylindrical bars, made of an incompressible strain hardening plastic material, are investigated. A Lagrangian linear perturbation analysis is performed to obtain a fourth order partial differential equation which governs the evolution of the perturbation. The analysis shows that inertia slows down the growth of long wavelengths while bidimensional effects conjugated to strain hardening extinct short wavelengths. The present approach is applied successfully to the analysis of bifurcation and instabilities in (i) a rectangular block during plane strain extension, (ii) a circular bar during uniaxial extension. New results are obtained in the case of rate independent materials and a synthetical point of view is obtained for rate dependent behaviors.

Keywords: Bifurcation; Instability; Dynamic extension

1. Introduction

In rapid stretching, structures can develop a multiple necking pattern which leads to the fracture in several fragments. Experimental evidence of this phenomenon has been reported by several authors. Niordson (1965) has developed an experimental device in which an intense electromagnetic field is used to expand thin rings at high strain rate. In the loaded specimen, many necks are observed along the circumference. Grady and Benson (1983) performed dynamic expansion of aluminium and copper rings using the former technique. The authors enlight the enhanced ductility of metals in dynamic conditions compared to quasi-static conditions. They observed also the fragmentation of rings at high velocity testings. They have noted that the number of fragments increases with the loading velocity. More recently, Altynova et al. (1996) have also performed expansion of rings (Al, T6AL, Cu alloys) by electromagnetic means. Trends observed by Grady and Benson (1983) are retrieved by these authors. The fragmentation is also observed in axisymmetric jet formed by the collapse of a linear shaped liner under explosive loading. During the flight,

* Corresponding author. Tel.: +33-0-3-87-31-53-69; fax: +33-0-3-87-31-53-66.
E-mail address: molinari@lpmm.univ-metz.fr (A. Molinari).

0020-7683/02/$ - see front matter © 2002 Elsevier Science Ltd. All rights reserved.
doi:10.1016/S0020-7683(03)00020-9

the jet is stretched at high strain rate and fragments are sometimes observed (see Karpp and Simon, 1976; Chou et al., 1977).

Many contributions have been devoted to the analysis of bifurcation and instabilities occuring during plastic loading. Most of them were concerned by quasi-static situations. Hill and Hutchinson (1975) have developed a quasi-static bifurcation analysis for a rectangular plate subjected to plane strain tension. The material has a rate independent behavior. Depending on the deformation state, the bifurcation can occur in the elliptic, parabolic or hyperbolic regimes. Young (1976) carried out a similar analysis in plane strain compression. Benallal and Tvergaard (1995) examined the role of non local effects on bifurcation in the plane strain tension and compression tests.

Multiple necking during high strain rate loadings is the result of inertia effects. Therefore the above mentioned analyses have to be extended to account for inertia forces. Sorensen and Freund (1998) have extended the approach of Hill and Hutchinson (1975) in dynamic conditions. Acceleration term in the momentum balance is taken into account. But the hydrostatic pressure contribution resulting from lateral inertia is ignored so that this dynamic analysis is valid for large ratio of length to width of the block. The material is rate independent and the incompressibility assumption is adopted. The elliptic, hyperbolic and parabolic regimes are identical to those established by Hill and Hutchinson (1975). Owing to the inertia term in the momentum balance, the rate of growth of the bifurcation mode is evaluated. It is found that long wavelength modes are suppressed by inertia. Shenoy and Freund (1999) improved the previous work by taking into account of the hydrostatic pressure contribution due to the lateral inertia. In this analysis, the material behavior is rate independent with an isotropic hardening. By considering the rate of growth of perturbations, it is observed that a particular wavelength is selected which characterizes the size of the fragments. The authors claim that inertia is responsible for this phenomenon since they considered that inertia suppress both short and long wavelength mode of bifurcation. In addition the authors have enlightened the fact that the number of necks is not influenced by the level of strain hardening.

Ring experiments have also been modelled by finite element calculations. An interesting work has been performed by Han and Tvergaard (1995). The material is a rate independent elastic–plastic solid. A small imperfection triggers the onset of necking. Nevertheless, due to wave propagation, the number of necks can exceed the number of initial thin points introduced by the imperfection. The authors have shown that the neck spacing is dependent on the loading and on the aspect ratio of the cross section. On the contrary, the magnitude of the initial defect and of the strain hardening coefficient does not influence the necking pattern.

The previous works concern rate-independent material. For rate dependent material, the problem of a rectangular block subjected to tension has been analysed by Hutchinson et al. (1978). Using a linear perturbation analysis, the authors have concluded that the strain rate sensitivity effects damp short wavelengths. The effect of strain rate sensitivity has been already mentioned by Hutchinson and Neale (1977) in the long wavelength analysis of neck formation in a viscoplastic bar. To model fragmentation in viscoplastic solids, Fressengeas and Molinari (1994) have extended the previous work by adding inertial effects. It was demonstrated that inertia slows down the growth of long wavelengths. This role in combination with the stabilizing aspects of viscosity and of bidimensional effects on short wavelengths leads to the selection of an intermediate wavelength (the fastest growing mode). Note that the fastest growing mode is time dependent. The role of inertia was already mentioned by Fressengeas and Molinari (1985). An extension of the theory proposed by Fressengeas and Molinari (1994) has been carried out by Jeanclaude and Fressengeas (1997). They analysed the fragmentation of a rapidly stretching bar in an axisymmetric loading. This bidimensional dynamic analysis has provided similar results (selection of an intermediate wavelength due to inertia and strain rate sensitivity).

In this paper, a theoretical analysis of dynamic bifurcation of a cylindrical bar is performed. The material is incompressible rate insensitive with strain hardening. Owing to a linear perturbation analysis, the rate of growth of the perturbation is evaluated. Various stabilizing effects delay the growth of disturbances. Inertia slows down the long wavelengths whereas bidimensional effects damp the short wavelengths.

The paper is organized as follows. In Section 2, the linear stability analysis is developed for a cylindrical bar and a rate insensitive hardening material. In Section 3, an extension of the contribution of Shenoy and Freund (1999) for the dynamic bifurcation of a rectangular block (rate insensitive materials) is proposed in a Lagrangian frame. Next, the dynamic instability of cylindrical bars and rectangular sheets for rate sensitive materials is presented in Section 4. Comparisons are carried out with published results (Fressengeas and Molinari, 1994; Jeanclaude and Fressengeas, 1997). Finally, in Section 5, new results are proposed for a cylindrical bar made of a rate insensitive material with strain hardening.

2. Rate insensitive material under axisymmetric loading

Since an axisymmetric problem is considered here, the cylindrical coordinate system is adopted, associated to the frame $(\mathbf{e_r}, \mathbf{e_\theta}, \mathbf{e_z})$. The Lagrangian coordinates of a material point are noted (R, θ, Z). The cylinder occupies in the undeformed state the region $-L_0 < Z < L_0$ and $0 \leqslant R \leqslant R_0$, where $2L_0$ is the initial length of the bar, R_0 is the initial radius. The body is subjected to uniform velocity $\pm V_0\mathbf{e_z}$ applied at the extremities $Z = \pm L_0$ (see Fig. 1). In the deformed state at current time t, the position of a particle is given by

$$r = r(R, Z, t) \quad z = z(R, Z, t) \tag{1}$$

The material is assumed incompressible, rate independent with strain hardening. The behavior is defined by the constitutive law developed by Stören and Rice (1975). In axisymmetric loading, the Jaumann rate $\hat{\boldsymbol{\sigma}}$ of the Cauchy stress tensor $\boldsymbol{\sigma}$ is:

$$\hat{\sigma}_{rr} = (\mu^* + \mu)D_{rr} - (\mu - \mu^*)D_{\theta\theta} - \dot{p} \tag{2a}$$

$$\hat{\sigma}_{\theta\theta} = (\mu^* + \mu)D_{\theta\theta} - (\mu - \mu^*)D_{rr} - \dot{p} \tag{2b}$$

$$\hat{\sigma}_{zz} = 2\mu^* D_{zz} - \dot{p} \quad \hat{\sigma}_{ij} = 2\mu D_{ij} \quad \text{for } i \neq j \tag{2c}$$

$\boldsymbol{D}$ is the strain rate tensor. μ^* and μ are the moduli defined by:

$$\mu^* = \frac{1}{3}\frac{\partial\sigma_e}{\partial\epsilon_e} \quad \mu = \frac{1}{3}\frac{\sigma_e}{\epsilon_e} \tag{3}$$

where $\sigma_e = (3/2\mathbf{s} : \mathbf{s})^{1/2}$ is the effective stress and $\mathbf{s}$ is the deviator of the Cauchy stress tensor. The effective strain is defined by $\epsilon_e = \int D_e \, dt$, with $D_e = (2/3\mathbf{D} : \mathbf{D})^{1/2}$ being the effective strain rate. Furthermore, the hardening behavior is specified by the Hollomon's law (1945):

$$\sigma_e = \sigma_0 \epsilon_e^n \tag{4}$$

with n the strain hardening exponent, σ_0 a scaling factor.

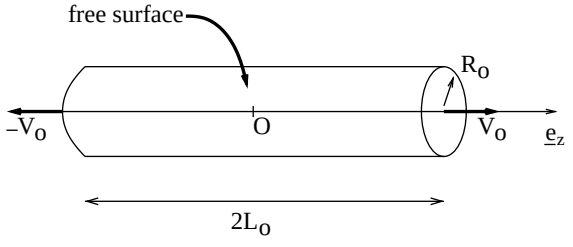

Fig. 1. View of the cylindrical bar, of initial length $2L_0$ and of initial radius R_0. Velocities $\pm V_0$ are applied at the extremities $Z = \pm L_0$. The lateral surface $R = R_0$ is traction free.

The boundary conditions of the problem are, respectively at the extremities $Z = \pm L_0$ and at the lateral surface $R = R_0$:

$$T_{zr}(R, Z = \pm L_0, t) = 0 \quad T_{z\theta}(R, Z = \pm L_0, t) = 0 \quad v_z(R, Z = \pm L_0, t) = \pm V_0 \tag{5a}$$

$$T_{rr}(R_0, Z, t) = 0 \quad T_{r\theta}(R_0, Z, t) = 0 \quad T_{rz}(R_0, Z, t) = 0 \tag{5b}$$

where $\mathbf{T}$ is the nominal stress tensor related to the Cauchy stress tensor $\boldsymbol{\sigma}$ by:

$$\mathbf{T} = \boldsymbol{F}^{-1} \cdot \boldsymbol{\sigma} \tag{6}$$

with $\boldsymbol{F}$ being the gradient of the deformation. The incompressibility condition ($\det \boldsymbol{F} = 1$) has been used. The traction vector $\mathbf{t}$, acting at the point across the surface whose outward normal is $\mathbf{n}$, has been defined as in Malvern's book (1969) : $\mathbf{t} = \mathbf{n} \cdot \mathbf{T}$ ($t_i = n_j T_{ji}$). In the following, all mechanical quantities and operators are defined as in Malvern's book (1969).

The homogeneous deformation is given by Jeanclaude and Fressengeas (1997):

$$z = Z/\epsilon' \quad v_z^0 = \frac{V_0}{L_0} Z \tag{7a}$$

$$r = R\sqrt{\epsilon'} \quad v_r^0 = -\frac{1}{2}\frac{V_0}{L_0} R(\epsilon')^{3/2} \tag{7b}$$

with

$$\epsilon' = \frac{1}{1 + (V_0/L_0)t} \tag{8}$$

The corresponding Cauchy stress is:

$$[\boldsymbol{\sigma}_0] = \begin{bmatrix} -p^{\mathrm{I}} & 0 & 0 \\ 0 & -p^{\mathrm{I}} & 0 \\ 0 & 0 & \sigma_{\mathrm{e}}^0 - p^{\mathrm{I}} \end{bmatrix}_{R\theta Z} \tag{9}$$

p^{I} is the inertial pressure due to lateral deformation and σ_{e}^0 the background effective stress. By verifying the equation of motion and the boundary conditions, it is straightforward to obtain p^{I}:

$$p^{\mathrm{I}} = \frac{3}{8}\left(\frac{V_0}{L_0}\right)^2 \rho(\epsilon')^3 (R_0^2 - R^2) \tag{10}$$

with ρ the mass density.

In the following, the linear stability of the homogeneous deformation is investigated so as to determine the wavelength of the perturbation associated to the fastest growth rate.

2.1. Linear perturbation analysis

The analysis of the linear stability of the homogeneous solution defined by the relationships (7)–(10) is performed in a Lagrangian formulation. A perturbation in velocity $\boldsymbol{\delta v}$, respecting the axisymmetry of the problem, is added to the background field at a given time t_0, without any initial disturbance of the acceleration. Then

$$\boldsymbol{v} = \boldsymbol{v}^0 + \boldsymbol{\delta v} \quad \boldsymbol{\gamma} = \boldsymbol{\gamma}^0 + \boldsymbol{\delta \gamma} \tag{11}$$

with $\boldsymbol{\delta v}(t_0) = 0$, $\boldsymbol{\delta v}(t_0^+) \neq 0$ and $\boldsymbol{\delta \gamma}(t_0) = \boldsymbol{\delta \gamma}(t_0^+) = 0$. The validity of this assumption will be discussed in Section 2.2.4. Since the material is rate independent and the acceleration is not modified at time t_0^+, the background nominal stress tensor $\boldsymbol{T}_o$ satisfies the momentum equation at time t_0 and t_0^+:

$$\mathbf{Div}\, \boldsymbol{T}_0 = \rho \dot{\boldsymbol{v}} \tag{12}$$

where $(\cdot)$ is the material time derivative. Note that a perturbation in velocity and in acceleration added to the homogeneous background solution would imply a perturbation of the nominal stress tensor to respect the momentum equation (12).

The initial evolution of the velocity disturbance is sought using an incremental formulation. The rate of the momentum equation is:

$$\mathbf{Div}\, \dot{\boldsymbol{T}} = \rho \ddot{\boldsymbol{v}} \tag{13}$$

where **Div** is the Lagrangian divergence operator. The velocity gradient $\boldsymbol{L} = \dot{\boldsymbol{F}} \cdot \boldsymbol{F}^{-1}$ can be written at time t_0 and t_0^+ as:

$$[\boldsymbol{L}]_{R\theta Z} = \begin{bmatrix} \dfrac{1}{\sqrt{\epsilon'}} \dfrac{\partial v_r}{\partial R} & 0 & \epsilon' \dfrac{\partial v_r}{\partial Z} \\ 0 & \dfrac{v_r}{\sqrt{\epsilon'} R} & 0 \\ \dfrac{1}{\sqrt{\epsilon'}} \dfrac{\partial v_z}{\partial R} & 0 & \epsilon' \dfrac{\partial v_z}{\partial Z} \end{bmatrix} \tag{14}$$

In calculating (14), we have used the fact that $\boldsymbol{F}(t_0^+) = \boldsymbol{F}(t_0) = \boldsymbol{F}_0$ (background solution) since a perturbation in velocity (and not in position) is considered.

Using the incompressibility condition $\det \boldsymbol{F} = 1$, the rate of the nominal stress, obtained by time derivation of Eq. (6), is related to the Jaumann rate of the Cauchy stress $\hat{\boldsymbol{\sigma}}$, for $t \leqslant t_0^+$:

$$\dot{\boldsymbol{T}} = \boldsymbol{F}_0^{-1} \cdot (\hat{\boldsymbol{\sigma}} - \boldsymbol{D} \cdot \boldsymbol{\sigma}_0 - \boldsymbol{\sigma}_0 \cdot \boldsymbol{\Omega}) \tag{15}$$

with $\boldsymbol{\Omega}$ the spin tensor. $\boldsymbol{\sigma}_0$ is the background stress tensor since the acceleration is not perturbed at time t_0^+.

According to relationships (2), (9), (14) and (15), the non zero components of $\dot{\boldsymbol{T}}$ are:

$$\dot{T}_{rr} = (\mu^* + \mu + p^{\mathrm{I}}) \frac{v_{r,R}}{\epsilon'} - (\mu - \mu^*) \frac{v_r}{\epsilon' R} - \frac{\dot{p}}{\sqrt{\epsilon'}} \tag{16a}$$

$$\dot{T}_{rz} = \left(\mu - \frac{\sigma_{\mathrm{e}}^0}{2} + p^{\mathrm{I}}\right) \sqrt{\epsilon'} v_{r,Z} + \left(\mu - \frac{\sigma_{\mathrm{e}}^0}{2}\right) \frac{v_{z,R}}{\epsilon'} \tag{16b}$$

$$\dot{T}_{\theta\theta} = -(\mu - \mu^*) \frac{v_{r,R}}{\epsilon'} + (\mu^* + \mu + p^{\mathrm{I}}) \frac{v_r}{\epsilon' R} - \frac{\dot{p}}{\sqrt{\epsilon'}} \tag{16c}$$

$$\dot{T}_{zr} = \left(\mu + \frac{\sigma_{\mathrm{e}}^0}{2}\right) \epsilon'^2 v_{r,Z} + \left(\mu - \frac{\sigma_{\mathrm{e}}^0}{2} + p^{\mathrm{I}}\right) \sqrt{\epsilon'} v_{z,R} \tag{16d}$$

$$\dot{T}_{zz} = (2\mu^* - \sigma_{\mathrm{e}}^0 + p^{\mathrm{I}}) \epsilon'^2 v_{z,Z} - \epsilon' \dot{p} \tag{16e}$$

where the comma stands for the partial derivative, as for instance, $(\ )_{,R} = \partial(\ )/\partial R$. $\dot{\boldsymbol{T}}$ must satisfy the momentum equation (13). Cross-differentiating the obtained relationships so as to eliminate the rate of pressure $\dot{p} = -(1/3)\mathrm{tr}\,(\dot{\boldsymbol{\sigma}})$ and using the incompressibility condition

$$\mathrm{tr}\boldsymbol{D} = 0 \quad \text{or} \quad \frac{v_{r,R}}{\sqrt{\epsilon'}} + \frac{v_r}{\sqrt{\epsilon'} R} + \epsilon' v_{z,Z} = 0, \tag{17}$$

a single partial differential equation is found for $t \leqslant t_0^+$:

$$\frac{1}{\sqrt{\epsilon'}}\left(\mu^* + \frac{\sigma_e^0}{2}\right)\left(v_{r,RRZ} + \frac{v_{r,RZ}}{R} - \frac{v_{r,Z}}{R^2}\right) + \left(\mu + \frac{\sigma_e^0}{2}\right)\epsilon'^{\frac{5}{2}} v_{r,ZZZ} + \left(\mu - 2\mu^* + \frac{\sigma_e^0}{2}\right)\epsilon' v_{z,RZZ}$$
$$- \left(\mu - \frac{\sigma_e^0}{2}\right)\frac{1}{\epsilon'^2}\left(v_{z,RRR} + \frac{v_{z,RR}}{R} - \frac{v_{z,R}}{R^2}\right) - p^{\mathrm{I}}_{,RR}\frac{v_{r,Z}}{\sqrt{\epsilon'}} = \rho\left(\ddot{v}_{r,Z}\sqrt{\epsilon'} - \frac{\ddot{v}_{z,R}}{\epsilon'}\right) \tag{18}$$

It is noteworthy that the background velocity field (7) satisfies both incompressibility (17) and Eq. (18). Considering the expressions (17) and (18) at time t_0 and t_0^+ and the linear dependence with respect to $\boldsymbol{v}$, the perturbation $\delta\boldsymbol{v}$ at time t_0^+ is found to satisfy Eqs. (17) and (18).

A stream function $\Phi(R, Z, t)$ is introduced such that the perturbed velocity is:

$$\delta v_r = \frac{\sqrt{\epsilon'}}{R}\frac{\partial \Phi}{\partial Z} \quad \delta v_z = -\frac{1}{R\epsilon'}\frac{\partial \Phi}{\partial R} \tag{19}$$

It follows that the incompressibility condition (17) is automatically satisfied. By substitution of Eq. (19) into Eq. (18), a fourth order partial differential equation governing the evolution of Φ is obtained:

$$(\mu - 3\mu^*)\left(\frac{\Phi_{,RZZ}}{R^2} - \frac{\Phi_{,RRZZ}}{R}\right) + \left(\mu + \frac{\sigma_e^0}{2}\right)\epsilon'^3\frac{\Phi_{,ZZZZ}}{R}$$
$$- \left(\mu - \frac{\sigma_e^0}{2}\right)\frac{1}{\epsilon'^3}\left(\frac{3}{R^4}\Phi_{,R} - \frac{3}{R^3}\Phi_{,RR} + \frac{2}{R^2}\Phi_{,RRR} - \frac{1}{R}\Phi_{,RRRR}\right)$$
$$= \rho\left(\epsilon'\frac{\ddot{\Phi}_{,ZZ}}{R} - \frac{1}{\epsilon'^2}\left(\frac{\ddot{\Phi}_{,R}}{R^2} - \frac{\ddot{\Phi}_{,RR}}{R}\right) - \frac{V_0}{L_0}\left(\epsilon'^2\frac{\dot{\Phi}_{,ZZ}}{R} + \frac{2}{\epsilon'}\left(\frac{\dot{\Phi}_{,R}}{R^2} - \frac{\dot{\Phi}_{,RR}}{R}\right)\right)\right) \tag{20}$$

The perturbed boundary conditions, derived from the relationships (5) are

$$\delta v_z(R, \pm L_0, t) = 0, \quad \delta\dot{T}_{zr}(R, \pm L_0, t) = 0 \tag{21a}$$

$$\delta\dot{T}_{rr}(R_0, Z, t) = 0, \quad \delta\dot{T}_{rz}(R_0, Z, t) = 0 \tag{21b}$$

Using the definition of the velocity in terms of the stream function (19) and Eq. (16), the following conditions at $Z = \pm L_0$ are obtained:

$$\frac{\partial \Phi}{\partial R} = 0, \quad \left(\mu + \frac{\sigma_e^0}{2}\right)\frac{\epsilon'^3\Phi_{,zz}}{R} + \left(\mu + p^{\mathrm{I}} - \frac{\sigma_e^0}{2}\right)\left(\frac{\Phi_{,R}}{R^2} - \frac{\Phi_{,RR}}{R}\right) = 0 \tag{22}$$

and for $R = R_0$:

$$\epsilon'^3\Phi_{,zz} + \left(\frac{\Phi_{,R}}{R} - \Phi_{,RR}\right) = 0 \tag{23a}$$

$$\left(\mu - \frac{\sigma_e^0}{2}\right)\frac{1}{\epsilon'^2}\left(-\frac{\Phi_{,R}}{R^3} + \frac{\Phi_{,RR}}{R^2} - \frac{\Phi_{,RRR}}{R}\right) - \left(3\mu^* - \frac{\sigma_e^0}{2}\right)\epsilon'\frac{\Phi_{,RZZ}}{R} + 2\mu\epsilon'\frac{\Phi_{,ZZ}}{R^2} - \frac{3}{4}\left(\frac{V_0}{L_0}\right)^2\rho\epsilon'^4\Phi_{,ZZ}$$
$$+ \rho\left(2\frac{V_0}{L_0}\frac{\dot{\Phi}_{,R}}{R} + \frac{\ddot{\Phi}_{,R}}{R\epsilon'}\right) = 0 \tag{23b}$$

2.2. Axisymmetric mode

The purpose of this work is to evaluate the possibility of axisymmetric multiple necking in dynamic loading. Additional conditions along the centreline are necessary to respect axisymmetry:

$$\delta v_r(0,Z,t)=0 \quad \delta \dot{T}_{rz}(0,Z,t)=0 \tag{24}$$

Therefore, to satisfy (24) perturbation modes are searched of the form:

$$\Phi(R,Z,t)=AR\mathrm{e}^{\eta t}\sin(kZ)I_1(lR) \tag{25}$$

where k and l are respectively the Lagrangian longitudinal and radial wavenumbers; η is the growth rate of the perturbation, which is a real number (see Appendix A). In the following, the frozen coefficient theory is adopted which implies that the parameters k and l are considered as time independent. The mode is stable (resp. unstable) when $\eta<0$ (resp. $\eta>0$). I_1 represents the modified Bessel function of the first order. A is an amplitude factor. Note that the boundary conditions (22) are satisfied as soon as

$$kL_0=p\pi \tag{26}$$

where p is an integer which determines the number of initial thin points induced by the perturbation.

The substitution of (25) into (20) leads to a fourth order algebraic equation for the radial wavenumber l:

$$\left(\mu-\frac{\sigma_{\mathrm{e}}^0}{2}\right)\frac{l^4}{\epsilon'^3}+\left((\mu-3\mu^*)k^2-\rho\frac{\eta^2}{\epsilon'^2}-2\rho\frac{V_0}{L_0}\frac{\eta}{\epsilon'}\right)l^2+k^4\left(\mu+\frac{\sigma_{\mathrm{e}}^0}{2}\right)\epsilon'^3+\rho\epsilon' k^2\eta^2-\rho\frac{V_0}{L_0}\epsilon'^2k^2\eta=0 \tag{27}$$

As discussed by Hill and Hutchinson (1975), three different regimes exist: the elliptic domain where no roots are reals, the parabolic domain with two real roots and the hyperbolic one with four real roots. These regimes are analysed in the following.

2.2.1. Elliptic domain

2.2.1.1. Four complex roots. The four complex roots of Eq. (27) are noted

$$\pm l_1^{\mathrm{c}}(\eta,k), \quad \pm l_2^{\mathrm{c}}(\eta,k) \quad \text{with} \quad l_2^{\mathrm{c}}=\overline{l}_1^{\mathrm{c}} \tag{28}$$

where $\overline{(\cdot)}$ designates the conjugate of the complex number $(\cdot)$.

The perturbed stream function Φ has to be real; therefore Φ has the form:

$$\Phi=R\mathrm{e}^{\eta t}\sin(kZ)\{AI_1(l_1^{\mathrm{c}}R)+\overline{A}I_1(\overline{l}_1^{\mathrm{c}}R)\} \tag{29}$$

The perturbated stream function must satisfy the boundary conditions (23). This provides two relationships:

$$\mathscr{R}_{\mathrm{e}}\{AX_1(l_1^{\mathrm{c}})\}=0 \quad \mathscr{R}_{\mathrm{e}}\{AX_2(l_1^{\mathrm{c}})\}=0 \tag{30}$$

The notation $\mathscr{R}_{\mathrm{e}}\{\cdot\}$ represents the real part of the complex number $\{\cdot\}$. The expression $X_1(l)$, obtained from (23a), has the following form:

$$X_1(l)=\left(k^2\epsilon'+\left(\frac{l}{\epsilon'}\right)^2\right)I_1(lR_0) \tag{31}$$

and $X_2(l)$, deduced from (23b), is:

$$X_2(l) = -\frac{\mu - \frac{\sigma_e^0}{2}}{\epsilon'^2}\left(l^3 I_1'(lR_0) + \frac{l^2 I_1(lR_0)}{R_0}\right) - 2\mu\epsilon' k^2 \frac{I_1(lR_0)}{R_0} + \left(3\mu^* - \frac{\sigma_e^0}{2}\right)\epsilon' \frac{k^2}{R_0}(I_1(lR_0) + R_0 l I_1'(lR_0)) + \frac{3}{4}\left(\frac{V_0}{L_0}\right)^2 \rho\epsilon'^4 k^2 R_0 I_1(lR_0) + \rho\left[\frac{2V_0}{L_0 R_0}\eta(I_1(lR_0) + R_0 l I_1'(lR_0)) + \frac{\eta^2}{R_0\epsilon'}(I_1(lR_0) + R_0 l I_1'(lR_0))\right] \tag{32}$$

I_1' represents the derivative of the Bessel function I_1. The two conditions (30) are valid for any amplitude factor A and merge into an unique relationship after elimination of the complex number A:

$$\mathscr{I}_m\{X_1(l_1^c)\overline{X}_2(l_1^c)\} = 0 \tag{33}$$

where $\mathscr{I}_m\{\cdot\}$ designates the imaginary part of the complex number $\{\cdot\}$. For a given wavenumber k, the growth rate of the perturbation η is solution of Eq. (33).

2.2.1.2. Four purely imaginary roots. The four roots are supposed to be purely imaginary and are noted $\pm \mathrm{i} l_1^i(\eta, k)$, $\pm \mathrm{i} l_2^i(\eta, k)$, where i is the complex number defined by $\mathrm{i}^2 = -1$. In this regime, the necessary form for the perturbed stream function Φ is:

$$\Phi = R\mathrm{e}^{\eta t}\sin(kZ)[\mathrm{i}B_1 I_1(\mathrm{i}l_1^i R) + \mathrm{i}B_2 I_1(\mathrm{i}l_2^i R)] \tag{34}$$

B_1 and B_2 are real amplitude factors. As before, from the boundary conditions (23) an equation for the rate of growth η is found:

$$X_1(\mathrm{i}l_1^i)X_2(\mathrm{i}l_2^i) - X_1(\mathrm{i}l_2^i)X_2(\mathrm{i}l_1^i) = 0 \tag{35}$$

2.2.2. Parabolic domain

Two roots are real, noted $\pm l_1^p(\eta, k)$; the two others are purely imaginary, noted $\pm \mathrm{i} l_2^p(\eta, k)$. The necessary form for the stream function Φ is

$$\Phi = R\mathrm{e}^{\eta t}\sin(kZ)[B_1 I_1(l_1^p R) + \mathrm{i}B_2 I_1(\mathrm{i}l_2^p R)] \tag{36}$$

B_1 and B_2 are still real amplitude factors. Since Eq. (23) must be satisfied for any B_1 and B_2, the equation governing the rate of growth of the perturbation η is given by:

$$X_1(l_1^p)X_2(\mathrm{i}l_2^p) - X_1(\mathrm{i}l_2^p)X_2(l_1^p) = 0 \tag{37}$$

2.2.3. Hyperbolic domain

The four roots of Eq. (27) are real, noted $\pm l_1^h(\eta, k)$, $\pm l_2^h(\eta, k)$. The stream function Φ has the following form:

$$\Phi = R\mathrm{e}^{\eta t}\sin(kZ)[B_1 I_1(l_1^h R) + B_2 I_1(l_2^h R)] \tag{38}$$

Owing to the boundary conditions (23), η is solution of:

$$X_1(l_1^h)X_2(l_2^h) - X_1(l_2^h)X_2(l_1^h) = 0 \tag{39}$$

2.2.4. Discussions

The regime in which bifurcation occurs, depends on the size of the bar (L_0, R_0), on the material behavior and on the loading history. It is shown in Appendix A that for each longitudinal wavenumber k, two growth rates η_1 and η_2 can be found. Thus two possible modes for the perturbation can exist:

$$\Phi^{(1,2)} = e^{\eta_{(1,2)}t}\sin(kZ)f_{(1,2)}(R) \tag{40}$$

Note that all boundary conditions (22) and (23) are satisfied by the two stream functions $\Phi^{(1,2)}$. The last condition to fulfill is the zero initial value of the perturbed acceleration vector. In our approach, this condition cannot be satisfied rigorously, because the radial dependency of the stream function is expanded with only one trial function. If an infinite number of appropriate trial functions $(I_n, n \geqslant 1)$ was used, the condition $\boldsymbol{\delta\gamma} = 0$ would be exactly satisfied. In the present analysis, the authors have kept only the fundamental term in the expansion serie. General treatments might be done as in heat transfer problem; see Ozisik (1968). However, it is seen in Appendix B, by linear combination of the two possible modes Φ^1 and Φ^2, that $\boldsymbol{\delta\gamma} = 0$ at time t_0^+ can be approached with good accuracy for bifurcation modes with large growth rate. In Section 5, only the most unstable mode of perturbation is presented.

Note that the proposed linear stability analysis evaluates the instantaneous growth rate of a perturbation associated to a wavenumber k. Since the governing equations for the stream function Φ are time dependent, so is the growth rate η. Then a perturbation can be unstable at a given time and stable at a later time (or the contrary). An instantaneous positive growth rate for the perturbation k at a given time is not a proof of the long term instability of this perturbation. Nevertheless, it will be seen in Section 5, that such approach can provide useful informations concerning the dynamic necking of cylindrical bars.

3. Rate insensitive material under plane strain loading

The bifurcation analysis of a rectangular plate, in dynamic plane strain extension, has been studied by Shenoy and Freund (1999) when the material has a rate insensitive behavior. These authors did not perform a full Lagrangian analysis, since, at each step of the deformation, the current configuration is taken as the reference. In this section, a full Lagrangian solution to this problem is proposed and compared with results of Shenoy and Freund (1999). A cartesian coordinate system is adopted, associated to the frame $(\mathbf{e_x}, \mathbf{e_y}, \mathbf{e_z})$. The Lagrangian coordinates of a particle are X_1, X_2. The body occupies the region $-L_1 \leqslant X_1 \leqslant L_1$ and $-L_2 \leqslant X_2 \leqslant L_2$ and is stretched with the velocity $\pm V_0\mathbf{e_x}$ at $X_1 = \pm L_1$, under plane strain conditions. The constitutive law is given by Stören and Rice (1975):

$$\hat{\sigma}_{11} = 2\mu^* D_{11} - \dot{p} \quad \hat{\sigma}_{22} = 2\mu^* D_{22} - \dot{p} \quad \hat{\sigma}_{12} = 2\mu D_{12} \tag{41}$$

μ and μ^* are defined by Eq. (3). The hardening is governed by (4).

The homogeneous solution is given by Fressengeas and Molinari (1994):

$$x_1 = \frac{X_1}{\epsilon'} \quad x_2 = X_2\epsilon' \quad \text{with} \quad \epsilon' = \frac{1}{1 + \frac{V_0}{L_1}t} \tag{42}$$

The homogeneous Cauchy stress is

$$[\boldsymbol{\sigma}_0] = \begin{bmatrix} \sigma^0 - p^{\mathrm{I}} & 0 \\ 0 & -p^{\mathrm{I}} \end{bmatrix} \quad \text{with} \quad p^{\mathrm{I}} = \rho\left(\frac{V_0}{L_1}\right)^2 (l_2^2 - X_2^2)\epsilon'^4 \tag{43}$$

Due to the plane strain condition, σ^0 is related to the background effective stress σ_e^0 by $\sigma^0 = 2\sigma_e^0/\sqrt{3}$.

The homogeneous deformation is perturbed as in Section 2. A perturbation in velocity is added at time t_0, without any initial change in the acceleration field. In the following, the velocity field $\mathbf{v}$ is the sum of the homogeneous field and of a perturbation depending on (X_1, X_2). As a consequence, the velocity gradient $\boldsymbol{L}$, valid at time t_0 and t_0^+ is defined as:

$$[\boldsymbol{L}] = \begin{bmatrix} \epsilon' \dfrac{\partial v_1}{\partial X_1} & \dfrac{1}{\epsilon'} \dfrac{\partial v_1}{\partial X_2} \\ \epsilon' \dfrac{\partial v_2}{\partial X_1} & \dfrac{1}{\epsilon'} \dfrac{\partial v_2}{\partial X_2} \end{bmatrix} \tag{44}$$

The rate of the nominal stress tensor $\dot{\boldsymbol{T}}$ is expressed in terms of the velocity field with use of Eqs. (15), (41) and (44). $\dot{p}$ is eliminated by cross differentiation of the momentum equation:

$$\dot{T}_{ji,j} = \rho \dot{\gamma}_i \tag{45}$$

where the notation $(\cdot)_{,j}$ stands for the partial derivative $\partial(\cdot)/\partial X_j$. After some algebraic development similar to those of Section 2, and with use of the incompressibility condition:

$$\epsilon' \frac{\partial v_1}{\partial X_1} + \frac{1}{\epsilon'} \frac{\partial v_2}{\partial X_2} = 0 \tag{46}$$

a third order partial differential equation is obtained:

$$\left(\mu - \frac{\sigma^0}{2}\right) \frac{v_{1,222}}{\epsilon'^3} + (2\mu^* - \mu)\left(\epsilon' v_{1,112} - \frac{v_{2,122}}{\epsilon'}\right) - \left(\mu + \frac{\sigma^0}{2}\right) \epsilon'^3 v_{2,111} - \beta \frac{v_{2,1}}{\epsilon'} = \rho \left(\frac{\ddot{v}_{1,2}}{\epsilon'} - \epsilon' \ddot{v}_{2,1}\right) \tag{47}$$

The last two relationships are satisfied by both the homogeneous velocity and the perturbed velocity $\delta \mathbf{v}$. The following analysis is similar to that of Section 2. To satisfy (46), we introduce a perturbed stream function Φ such that:

$$\delta v_1 = -\frac{1}{\epsilon'} \Phi_{,2} \quad \delta v_2 = \epsilon' \Phi_{,1} \tag{48}$$

The relationship (47), describing the evolution of the perturbation, is written in terms of Φ:

$$\begin{aligned} &\left(\mu - \frac{\sigma^0}{2}\right) \frac{1}{\epsilon'^4} \Phi_{,2222} + 2(2\mu^* - \mu) \Phi_{,1122} + \left(\mu + \frac{\sigma^0}{2}\right) \epsilon'^4 \Phi_{,1111} \\ &\quad = \rho \left(\epsilon'^2 \ddot{\Phi}_{,11} + \frac{1}{\epsilon'^2} \ddot{\Phi}_{,22} + \frac{2V_0}{L_1 \epsilon'} \dot{\Phi}_{,22} - \frac{2V_0}{L_1} \epsilon'^3 \dot{\Phi}_{,11}\right) \end{aligned} \tag{49}$$

Note that Shenoy and Freund (1999) have analysed the same problem, assuming that the current configuration is the reference one. When adopting this assumption ($\epsilon' = 1$) in our formulation, the relationship (27) of Shenoy and Freund (1999) can not be retrieved. The difference is due to the rate of acceleration term obtained by time derivation of Eq. (48). In the proposed analysis, the time derivative of the term ϵ' is accounted for and modifies the expression (49) by the additional terms

$$\frac{2V_0}{L_1 \epsilon'} \dot{\Phi}_{,22} - \frac{2V_0}{L_1} \epsilon'^3 \dot{\Phi}_{,11}$$

The perturbed boundary conditions:

$$\delta v_1(\pm L_1, X_2, t) = 0 \quad \delta \dot{T}_{12}(\pm L_1, X_2, t) = 0 \tag{50a}$$

$$\delta \dot{T}_{21}(X_1, \pm L_2, t) = 0 \quad \delta \dot{T}_{22}(X_1, \pm L_2, t) = 0, \tag{50b}$$

can be expressed in terms of Φ. At $X_1 = \pm L_1$, we have

$$\Phi_2 = 0 \quad -\left(\mu + p^{\mathrm{I}} - \frac{\sigma^0}{2}\right) \frac{1}{\epsilon'} \Phi_{,22} + \epsilon'^3 \left(\mu + \frac{\sigma^0}{2}\right) \Phi_{,11} = 0 \tag{51}$$

and at the extremities $X_2 = \pm L_2$:

$$-\Phi_{,22} + \epsilon'^4 \Phi_{,11} = 0 \tag{52a}$$

$$\left(\frac{\sigma^0}{2} + \mu - 4\mu^*\right)\epsilon' \Phi_{,112} - \left(\mu - \frac{\sigma^0}{2}\right)\frac{1}{\epsilon'^3}\Phi_{,222} - \pm 2\rho\epsilon'^5 \frac{V_0^2 L_2}{L_1^2}\Phi_{,11} = -\rho\left(2\frac{V_0}{L_1}\dot{\phi}_{,2} + \frac{1}{\epsilon'}\ddot{\Phi}_{,2}\right) \tag{52b}$$

Only symmetric modes of bifurcation are considered in the current analysis. Additional relationships need to be checked to satisfy the symmetry:

$$\delta v_2(X_1, 0, t) = 0 \quad \delta \dot{T}_{21}(X_1, 0, t) = 0 \tag{53}$$

As in Fressengeas and Molinari (1994), the perturbed stream function Φ is chosen of the following form:

$$\Phi = A e^{\eta t} \sin(kX_1) \exp(\mathrm{i} l \epsilon'^2 X_2) \tag{54}$$

The substitution of (54) into (49) provides a fourth order algebraic equation for the transverse wavenumber l:

$$\left(\mu - \frac{\sigma^0}{2}\right) l^4 + \left((4\mu^* - 2\mu)k^2 + \rho\frac{\eta^2}{\epsilon'^2} + 2\rho\frac{V_0}{L_1}\frac{\eta}{\epsilon'}\right) l^2 + k^4\left(\mu + \frac{\sigma^0}{2}\right) + \frac{\rho}{\epsilon'^2}k^2\eta^2 - 2\rho\frac{V_0}{\epsilon' L_1}k^2\eta = 0 \tag{55}$$

As in the axisymmetric analysis, three different regimes (elliptic, parabolic and hyperbolic) can be investigated. The rate of growth of the perturbation η is found as the solution of a non linear equation resulting from the boundary conditions (52a) and (52b) and from the condition of symmetry (53). The details are not provided in the present paper (similar to Section 2). Note that, as in Appendix B, it can be shown that the initial condition of zero perturbed acceleration can be approached with good accuracy.

To capture the bifurcation rate η, Shenoy and Freund (1999) introduced the "necking rate" index N as the ratio of the rate of growth η to the background uniform strain rate V_0/L_1:

$$N = \frac{1}{2}\left(\frac{L_1\eta}{V_0}\right)^2 \tag{56}$$

Note that the bifurcation exists if the necking rate N is large compared to unity.

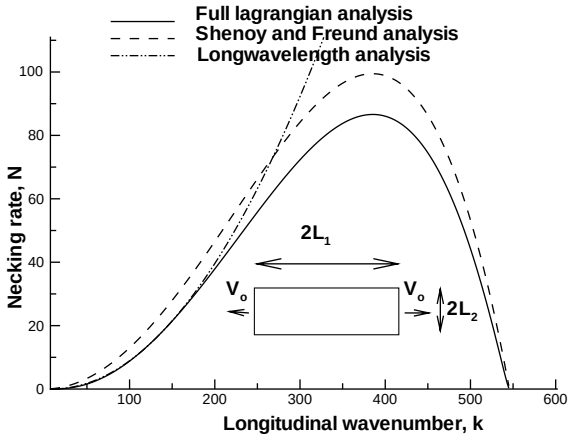

Fig. 2. Necking of a stretched plate. Evolution of the necking rate as a function of the longitudinal wavenumber k. The results are compared to those of Shenoy and Freund (1999) and to the long wavelength analysis. The material, rate insensitive with strain hardening, is representative of an OHFC copper: $\sigma_0 = 490$ MPa, $n = 0.4$ $\rho = 8900$ kg/m^3, $\epsilon_e = (2/\sqrt{3})n(1 + 0.0026)$. The configuration is $2L_1 = 100$ mm, $2L_2 = 2$ mm and $V_0 = \pm 33$ m/s.

For illustration, as in Shenoy and Freund (1999), the material considered is an OFHC copper whose properties have been reported by Altynova et al. (1996) ($\sigma_0 = 490$ MPa, $n = 0.4$, $\rho = 8900$ kg/m^3). The geometry of the plate is $2L_1 = 100$ mm and $2L_2 = 2$ mm (aspect ratio $L_2/L_1 = 0.01$) in order to be consistent with the size of rings used by Altynova et al. (1996). The current configuration is taken as reference ($\epsilon' = 1$). The velocity applied at the extremities of the plate is $V_0 = \pm 33$ m/s. The homogeneous effective strain in the plate is $\epsilon_e^0 = (2/\sqrt{3})n(1 + 0.0026)$. The present analysis is compared to results of Shenoy and Freund (1999, Fig. 2) and of the dynamic long wavelength analysis (see formula 3–11, Fressengeas and Molinari, 1985). It is observed on Fig. 2 that long wavelength perturbations are slowed down by inertia. The necking rate N is close to zero when the longitudinal wavenumber k is small. In Section 5, it is seen that the two dimensional effects are mostly responsible for the damping of short wavelength modes. As a consequence of the interplay between the stabilizing role of inertia and of 2D effects, a wavelength of maximum growth rate is selected. Compared to the analysis of Shenoy and Freund (1999), the necking rate N predicted by our approach is lower, due to additional terms in the rate of acceleration which enhance the influence of inertia.

4. Instability analysis for rate sensitive material

The aim of this section is to analyse the stability of the deformation of viscoplastic non-hardening materials for two loading conditions: plane strain and axisymmetric extensions. At a given time t_0, a time dependent perturbation is added to the position of the particle. This implies a disturbance in the velocity, in the acceleration and also in the stress tensor (since the material is rate dependent). In the following, the background position, velocity, Cauchy stress and nominal stress are noted $\mathbf{x}$, $\mathbf{v}$, $\boldsymbol{\sigma}$ and $\mathbf{T}$; the corresponding perturbed quantities are designated as $\boldsymbol{\delta x}$, $\boldsymbol{\delta v}$, $\boldsymbol{\delta\sigma}$ and $\boldsymbol{\delta T}$.

The viscoplastic behavior is described by the J_2 flow theory

$$s_{ij} = \frac{2}{3}\sigma_e \frac{D_{ij}}{d_e} \tag{57}$$

The effective Cauchy stress σ_e is linked to the effective strain rate d_e by a powerlaw:

$$\sigma_e = \sigma_0 d_e^m \tag{58}$$

where m is the strain rate sensitivity.

4.1. Plane strain problem

The background solution is defined by Eqs. (42) and (43). The perturbation of this solution is performed within a Lagrangian frame. The disturbance of the nominal stress is given by:

$$\boldsymbol{\delta T} = (\boldsymbol{F} + \boldsymbol{\delta F})^{-1} \cdot (\boldsymbol{\sigma} + \boldsymbol{\delta\sigma}) - \boldsymbol{F}^{-1} \cdot \boldsymbol{\sigma} \tag{59}$$

whose components are:

$$\delta T_{11} = \epsilon'\left(\delta s_{11} - \delta p - \epsilon'\left(\frac{2\sigma_e^0}{\sqrt{3}} - p^I\right)\delta x_{1,1}\right) \quad \delta T_{22} = \frac{1}{\epsilon'}\left(\delta s_{22} - \delta p + \frac{p^I}{\epsilon'}\delta x_{2,2}\right) \tag{60a}$$

$$\delta T_{21} = \frac{1}{\epsilon'}\left(\delta s_{21} - \epsilon'\left(\frac{2\sigma_e^0}{\sqrt{3}} - p^I\right)\delta x_{2,1}\right) \quad \delta T_{12} = \epsilon'\left(\delta s_{12} + \frac{p^I}{\epsilon'}\delta x_{1,2}\right) \tag{60b}$$

In plane strain conditions, the components of the perturbed Cauchy stress deviatoric tensor $\delta\mathbf{s}$ are obtained from (57):

$$\delta s_{11} = \frac{2m}{3}\frac{\sigma_e^0}{d_e^0}\delta D_{11} \quad \delta s_{22} = -\delta s_{11} \quad \delta s_{12} = \frac{2}{3}\frac{\sigma_e^0}{d_e^0}\delta D_{12} \tag{61}$$

The incompressibility condition ($\det \boldsymbol{F} = 1$) expressed in terms of the perturbation gives:

$$\epsilon' \frac{\partial \delta x_1}{\partial X_1} + \frac{1}{\epsilon'}\frac{\partial \delta x_2}{\partial X_2} = 0 \tag{62}$$

To satisfy (62), a stream function Φ is introduced such that:

$$\delta x_1 = -\frac{1}{\epsilon'}\Phi_{,2} \quad \delta x_2 = \epsilon' \Phi_{,1} \tag{63}$$

After elimination of the pressure perturbation δp in the perturbed momentum equation ($\mathrm{Div}\,\dot{\boldsymbol{\delta T}} = \rho \dot{\boldsymbol{\delta v}}$), we obtain by using the incompressibility condition (62) and the definition of the stream function (63), a fourth order partial differential equation for Φ:

$$\frac{\sigma_e^0}{3d_e^0}\left(\frac{1}{\epsilon'^4}\dot{\Phi}_{,2222} + \epsilon'^4 \dot{\Phi}_{,1111} - 2(1-2m)\dot{\Phi}_{,1122}\right) = \rho\left(\epsilon'^2 \ddot{\Phi}_{,11} + \frac{1}{\epsilon'^2}\ddot{\Phi}_{,22} + 2\frac{V_0}{L_1}\left(\frac{1}{\epsilon'}\dot{\Phi}_{,22} - \epsilon'^3 \dot{\Phi}_{,11}\right)\right) \tag{64}$$

The boundary conditions are $\delta v_1 = 0$ and $\delta T_{12} = 0$ for $X_1 = \pm L_1$, and $\delta T_{21} = 0$, $\delta T_{22} = 0$ for $X_2 = \pm L_2$. The last two conditions are written in terms of Φ:

$$\frac{\sigma_e^0}{3d_e^0}\left(\epsilon'^2 \dot{\Phi}_{,11} - \frac{1}{\epsilon'^2}\dot{\Phi}_{,22}\right) - \frac{2}{\sqrt{3}}\epsilon'^2 \sigma_e^0 \Phi_{,11} = 0 \tag{65a}$$

$$\frac{4m\epsilon'\sigma_e^0}{3d_e^0}\dot{\Phi}_{,112} - \frac{\sigma_e^0}{3d_e^0}\left(\epsilon'\dot{\Phi}_{,112} - \frac{\dot{\Phi}_{,222}}{\epsilon'^3}\right) \pm 2\rho\left(\frac{V_0}{L_1}\right)^2 \epsilon'^5 L_2 \Phi_{,11} = \rho\left(2\frac{V_0}{L_1}\dot{\Phi}_{,2} + \frac{1}{\epsilon'}\ddot{\Phi}_{,2}\right) \tag{65b}$$

Only symmetric instability modes are considered in the current analysis. So, additional conditions along the centreline need to be checked:

$$\delta v_2(X_1, 0, t) = 0 \quad \delta T_{21}(X_1, 0, t) = 0 \tag{66}$$

Finally, the stream function Φ is taken as in (54). Details are not presented here (similar as in Section 2). The growth rate of the perturbation η, for a given longitudinal wavenumber k, is obtained by combining (54), (64), (65) and (66). Since the material behavior is viscoplastic, it can be noted that instability occurs in the elliptic domain (see Fressengeas and Molinari, 1994).

To capture the evolution of the perturbation relative to the homogeneous background strain rate, a growth rate index G is defined (see Fressengeas and Molinari, 1994):

$$G = \frac{m\eta L_1}{V_0} \tag{67}$$

A dimensionless number I characterizing inertia effects relative to the viscoplastic effects is defined as:

$$I = \frac{\rho V_0^2}{\sigma_0\left(\frac{2}{\sqrt{3}}\right)^{m+1}\left(\frac{V_0}{l_1}\right)^m} \tag{68}$$

This problem has already been investigated by Fressengeas and Molinari (1994), using a different scheme. The main difference is the definition of the stream function using the incompressibility condition ($\det \boldsymbol{F} = 1$) rather than the other condition ($\overline{\det \boldsymbol{F}} = 0$). Therefore, in our approach, Φ is linked to the position. In Fressengeas and Molinari (1994), Φ is linked to the velocity. Moreover, in their approach, the rate of growth of the perturbation is solution of an ordinary differential equation. For illustration, the

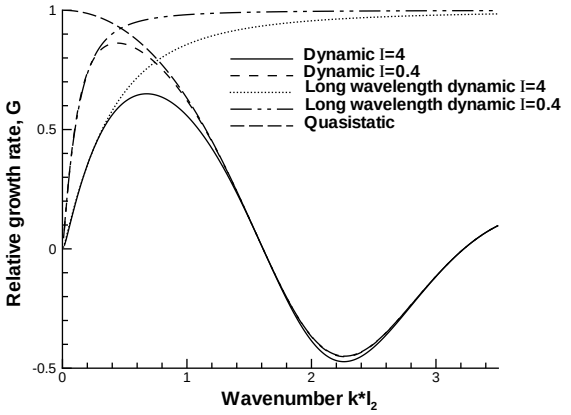

Fig. 3. Necking of a stretched plate. Effect of the dimensionless number I ($I = 4$ or $I = 0.4$) on the initial growth rate G. The results are compared to the long wavelength dynamic and to the quasi-static analyses. The present approach provides results identical to Fressengeas and Molinari (1994). The material (an OFHC copper) is viscoplastic without strain hardening: $\sigma_0 = 1.1010^8$ SI, $m = 0.05$ and $\rho = 8900$ kg/m^3. The configuration adopted is $L_1 = 0.03$ m and $L_2 = 0.01L_1$.

material behavior (representative of an OHFC copper) is defined by Eq. (58) with the following characteristics ($\sigma_0 = 1.110^8$ SI, $m = 0.05$, $\rho = 8900$ kg/m^3 (see Fressengeas and Molinari, 1994). The size of the plate is given by $L_1 = 0.03$ m and $L_2/L_1 = 0.01$. The results are presented in Fig. 3 for two values of I ($I = 4$ and $I = 0.4$). The results of the dynamic long wavelength (see formula 3–11, Fressengeas and Molinari, 1985) and of the quasi-static analyses are superimposed. The results provided by the present analysis are identical to those obtained previously by Fressengeas and Molinari (1994, Fig. 1). As noted by these authors, inertia slows down the long wavelengths. The short wavelengths are damped by the biaxial effects; the quasi-static and the dynamic approaches provide the same results for short wavelengths. The growth rate G is maximum for a finite wavelength, due to the interplay between inertia and viscous biaxial effects.

4.2. Axisymmetric problem

The homogeneous solution is defined by relationships (7)–(10). The perturbation of the nominal stress, given by Eq. (59), is expressed as:

$$\delta T_{rr} = \frac{1}{\sqrt{\epsilon'}}\left(\delta s_{rr} - \delta p + \frac{p^{\mathrm{I}}}{\sqrt{\epsilon'}}\delta x_{r,R}\right) \quad \delta T_{rz} = \frac{1}{\sqrt{\epsilon'}}(\delta s_{rz} - \epsilon'(\sigma_{\mathrm{e}}^0 - p^{\mathrm{I}})\delta x_{r,Z} \tag{69a}$$

$$\delta T_{\theta\theta} = \frac{1}{\sqrt{\epsilon'}}\left(\delta s_{\theta\theta} - \delta p + \frac{p^{\mathrm{I}}}{\sqrt{\epsilon'}}\frac{\delta x_r}{R}\right) \tag{69b}$$

$$\delta T_{zr} = \epsilon'\left(\delta s_{rz} + \frac{p^{\mathrm{I}}}{\sqrt{\epsilon'}}\delta x_{z,R}\right) \quad \delta T_{zz} = \epsilon'(\delta s_{zz} - \delta p - \epsilon'(\sigma_{\mathrm{e}}^0 - p^{\mathrm{I}})\delta x_{z,Z}) \tag{69c}$$

In axisymmetric loading, the perturbed deviatoric stress $\delta\mathbf{s}$ is defined by:

$$\delta s_{rr} = \frac{2}{3}\frac{\sigma_{\mathrm{e}}^0}{d_{\mathrm{e}}^0}\left(\delta D_{rr} - \frac{m-1}{2}\delta D_{zz}\right) \quad \delta s_{\theta\theta} = \frac{2}{3}\frac{\sigma_{\mathrm{e}}^0}{d_{\mathrm{e}}^0}\left(\delta D_{\theta\theta} - \frac{m-1}{2}\delta D_{zz}\right) \tag{70a}$$

$$\delta s_{zz} = \frac{2m}{3}\frac{\sigma_e^0}{d_e^0}\delta D_{zz} \quad \delta s_{ij} = \frac{2}{3}\frac{\sigma_e^0}{d_e^0}\delta D_{ij} \quad i \neq j \tag{70b}$$

The incompressibility condition ($\det \boldsymbol{F} = 1$)

$$\frac{\delta x_{r,R}}{\sqrt{\epsilon'}} + \frac{\delta x_r}{\sqrt{\epsilon'}R} + \epsilon' \delta x_{z,Z} = 0, \tag{71}$$

leads to the introduction of a stream function Φ such that the perturbed position is:

$$\delta x_r = \frac{\sqrt{\epsilon'}}{R}\frac{\partial \Phi}{\partial Z} \quad \delta x_z = -\frac{1}{R\epsilon'}\frac{\partial \Phi}{\partial R} \tag{72}$$

The pressure δp is eliminated by cross differentiation in the perturbed momentum equation. Using the incompressibility condition, a fourth order partial differential equation is obtained which governs the evolution of Φ:

$$\begin{aligned}\frac{\sigma_e^0}{3d_e^0}&\left((3m-1)\left(\dot{\Phi}_{,ZZRR} - \frac{\dot{\Phi}_{,ZZR}}{R}\right) + \epsilon'^3 \dot{\Phi}_{,ZZZZ} + \frac{1}{\epsilon'^3}\left(-3\frac{\dot{\Phi}_{,R}}{R^3} + 3\frac{\dot{\Phi}_{,RR}}{R^2} - 2\frac{\dot{\Phi}_{,RRR}}{R} + \dot{\Phi}_{,RRRR}\right)\right) \\ &= \rho\left[\epsilon'\ddot{\Phi}_{,ZZ} - \frac{1}{\epsilon'^2}\left(\frac{\ddot{\Phi}_{,R}}{R} - \ddot{\Phi}_{,RR}\right) - \frac{V_0}{L_0}\left(\epsilon'^2\dot{\Phi}_{,ZZ} + \frac{2}{\epsilon'}\left(\frac{\dot{\Phi}_{,R}}{R} - \dot{\Phi}_{,RR}\right)\right)\right]\end{aligned} \tag{73}$$

The stream function Φ is defined by Eq. (25). The boundary conditions valid at the extremities of the bar ($Z = \pm L_0$: $\delta v_z = 0$ and $\delta T_{zr} = 0$) are satisfied when $k = p(\pi/L_0)$. The two other boundary conditions ($\delta T_{rz} = 0$ and $\delta T_{zz} = 0$) valid at the outer radius ($R = R_0$), are written in terms of the stream function:

$$\ddot{\Phi}_{,ZZ} + \frac{1}{\epsilon'^3}\left(\frac{\dot{\Phi}_{,R}}{R} - \dot{\Phi}_{,RR}\right) - 3d_e^0\Phi_{,ZZ} = 0 \tag{74a}$$

$$\frac{2}{3}\frac{\sigma_e^0}{d_e^0}\left(-\frac{3m\epsilon'}{2}\frac{\dot{\Phi}_{,ZZR}}{R} + \epsilon'\frac{\dot{\Phi}_{,ZZ}}{R^2} - \frac{\dot{\Phi}_{,R}}{2\epsilon'^2R^3} + \frac{\dot{\Phi}_{,RR}}{2\epsilon'^2R^2} - \frac{\dot{\Phi}_{,RRR}}{2\epsilon'^2R}\right) - \frac{3}{4}\left(\frac{V_0}{L_0}\right)^2\rho\epsilon'^4\Phi_{,ZZ} + \rho\left(2\frac{V_0}{L_0}\frac{\dot{\Phi}_{,R}}{R} + \frac{\ddot{\Phi}_{,R}}{R\epsilon'}\right) \tag{74b}$$

Owing to viscosity, only an elliptic regim exists. The rate of growth η is obtained by combining (29), (73) and (74) (see Section 2).

This problem has already been investigated by Jeanclaude and Fressengeas (1997), using the method developed by Fressengeas and Molinari (1994) for the dynamic stretching of sheets. The present approach is more straightforward. A comparison between Jeanclaude and Fressengeas (1997) and the present approach is proposed on Fig. 4. The material is representative of an OHFC copper; the behavior is defined by Eq. (58) with the same properties as in the preceding section. The size of the cylindrical bar is given by $L_0 = 0.03$ m and $R_0/L_0 = 0.01$. The velocity at the tip is $V_0 = 300$ m/s. The effect of the strain rate sensitivity is investigated (see Fig. 4). Three different values of m are tested: $m = 0.05$, $m = 0.1$ and $m = 0.2$. As m becomes larger, the range where inertia has a significant influence decreases. Note that results in Fig. 4 are identical to those presented by Jeanclaude and Fressengeas (1997) in Fig. 2.

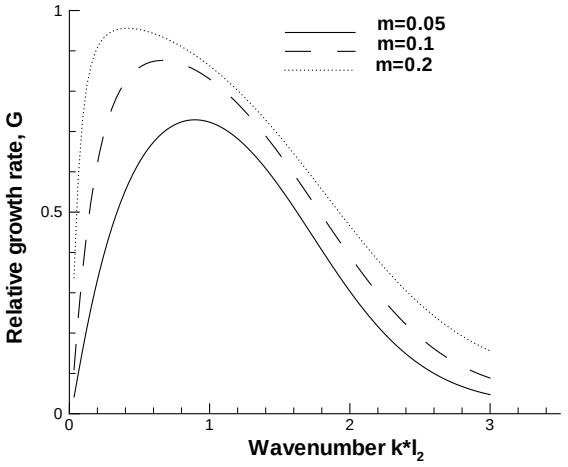

Fig. 4. Necking of a cylindrical bar. Effect of the strain rate sensitivity m on the initial relative growth rate G. The results are identical to Jeanclaude and Fressengeas (1997). The same material (viscoplastic without strain hardening) as in Fig. 3 is adopted. The configuration is $L_0 = 0.03$ m, $R_0 = 0.01L_0$ and $V_0 = 300$ m/s.

5. Results and discussions

We focus on the dynamic extension of a cylindrical bar (analysis developed in Section 2). The material is rate insensitive and strain hardening, representative of an OHFC copper. The hardening law is described by the relationship (4). The reference material properties are : $\sigma_0 = 490$ MPa, $n = 0.4$ and $\rho = 8900$ kg/m^3. The reference configuration is: $L_0 = 0.05$ m, $R_0/L_0 = 0.02$ and $V_0 = 33$ m/s. The cylindrical bar is initially prestrained by a given amount $\epsilon_e^0 = n$. The velocity V_0 is applied at the extremities $Z = \pm L_0$. The homogeneous effective strain at time t is:

$$\epsilon_e^0 = n + \ln\left(1 + \frac{V_0}{L_0}t\right) \tag{75}$$

The following calculations are carried out at the time $t = 23$ μs. A parametric study is performed in order to figure out the effects of inertia and of material properties on the necking rate N in the case of axisymmetric loadings.

In the Fig. 2, the comparison between the 2-D dynamic and the dynamic long wavelength 1-D analyses shows that inertia damps the long wavelength modes. The effect of the mass density on the necking rate N is visualized in Fig. 5. As ρ becomes larger, inertia effects increase. As a consequence, for a given longitudinal wavenumber k, the necking rate N decreases. Inertia acts as a stabilizing factor. Note that the Lagrangian wavelength of maximum growth is not depending on the mass density. The necking rate of short wavelengths (here $k > 550$) is still zero, whatever the mass density. The results of the Fig. 5 show that inertia is not responsible for the damping of short wavelengths. From Eqs. (27), (31) and (32), the parameters ρ and σ_0 can be merged into a ratio ρ/σ_0. Therefore the trends observed for σ_0 are the reverse of those previously observed for ρ. An increase of σ_0 leads to a higher necking rate (see Fig. 6), because the relative contribution of inertia is lowered by a larger σ_0.

To explain the damping of short wavelength perturbations, the radius of the cylindrical bar R_0 is varied, keeping constant all other parameters. The thinner the bar is, the higher is the necking rate and the shorter is the Lagrangian wavelength of maximum growth (see Fig. 7). The radius has a strong effect on the necking

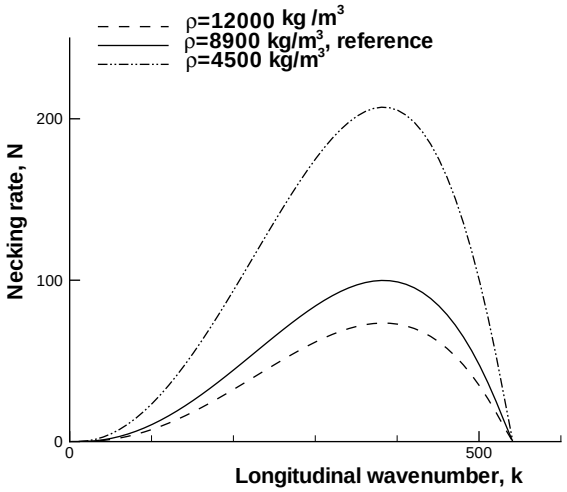

Fig. 5. Necking of a cylindrical bar. Influence of the mass density ρ on the necking rate N. The material is representative of a rate insensitive with strain hardening OFHC copper. The reference properties are $\sigma_0 = 490$ MPa, $n = 0.4$ and $\rho = 8900$ kg/m^3. The configuration is $L_0 = 0.05$ m, $R_0 = 0.02L_0$, $V_0 = 33$ m/s and $t = 23$ μs.

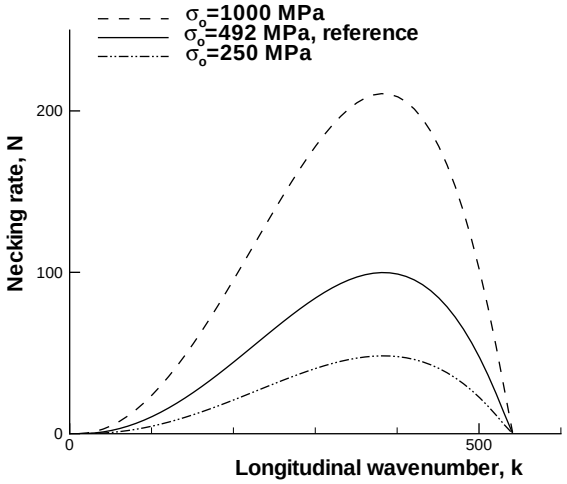

Fig. 6. Necking of a cylindrical bar. Influence of the stress level σ_0 on the necking rate N. The same reference for the material (rate insensitive with strain hardening) and the configuration as in Fig. 5 is considered.

rate of short wavelengths: for large values of R_0 short wavelength modes can not grow in the bar. Moreover, the radius does not have any influence on the necking rate of long wavelengths, since all curves present the same tangent at the origin.

The effect of the strain hardening is next investigated in Fig. 8. The strain hardening is a stabilizing factor since the necking rate N decreases as n becomes larger. Moreover, the Lagrangian wavelength of maximum growth is shifted to the domain of shorter wavelengths. As a consequence, the loss or extinction of short wavelength perturbations is mainly due to the multidimensional effects occuring in the necking zone which

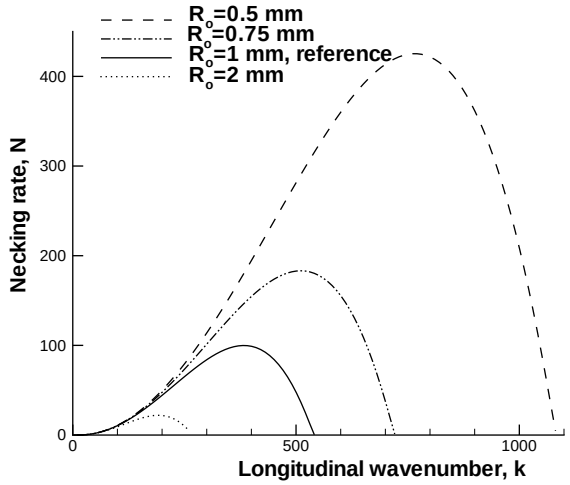

Fig. 7. Necking of a cylindrical bar. Influence of the radius R_0 on the necking rate N. The material is representative of a rate insensitive with strain hardening OFHC copper (see Fig. 5). The configuration is $L_0 = 0.05$ m, $V_0 = 33$ m/s and $t = 23$ μs.

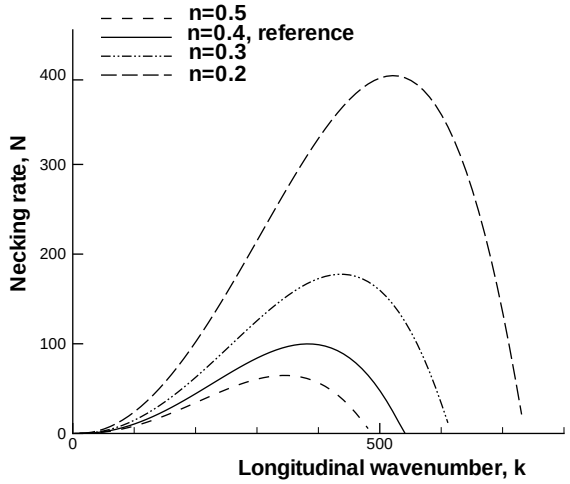

Fig. 8. Necking of a cylindrical bar. Effect of the strain hardening exponent n on the necking rate N. The same reference (rate insensitive material with strain hardening and configuration) as in Fig. 5 is adopted.

are interplaying with the stabilizing effects of strain hardening. To the authors' point of view, this refutes the claim of Shenoy and Freund (1999) that inertia is responsible of both damping of long and short wavelengths. Note that for a viscoplastic materials, Fressengeas and Molinari (1994) have concluded that inertia stabilizes the long wavelengths, while short wavelengths are damped by multiaxial effects.

Finally, the time evolution of the necking rate N is clearly depicted in Fig. 9. The Lagrangian wavelength of maximum growth evolves with time and is shifted to shorter wavelength. Therefore, a new mode of perturbation is dominant at each step of the deformation process. Calculations are performed for a

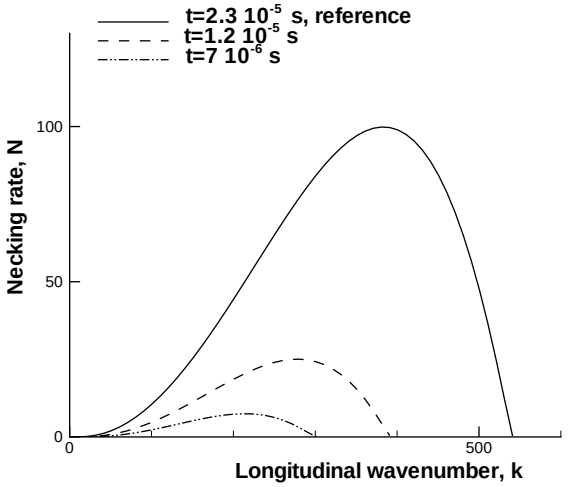

Fig. 9. Necking of a cylindrical bar. Time dependence of the necking rate N. Same rate insensitive material and same configuration are adopted as in Fig. 5.

homogeneous effective strain higher than n ($t \geqslant 0$ in Eq. (75)). The Considère criterion (1885) predicts the onset of instability for the effective strain being equal to n. Our calculations show that, due to inertia, 2-D effects and strain hardening, the growth rate of perturbations is rather weak just after the Considère criterion is reached, but gradually increases with time.

6. Conclusion

A Lagrangian analysis is proposed to characterize bifurcation or instability in dynamic loadings. The proposed method is an extension of the work of Hill and Hutchinson (1975) to the dynamic case. Improvements are given to the work of Shenoy and Freund (1999).

The necking bifurcation of a uniform cylindrical bar made of a rate insensitive hardening material is investigated through a linear perturbation analysis. It has been shown that inertia and strain hardening act as stabilizing factors. More precisely, inertia slows down the growth of long wavelength perturbations while multidimensional effects conjugated with strain hardening extinct short wavelength perturbations. The combination of these effects lead to the occurrence of a dominant mode. This dominant perturbation is time dependent so as at each moment, a different mode has the fastest growing rate.

The proposed method has also been applied to predict the development of instability in configuration such as rectangular sheet or cylindrical bar when the material is rate sensitive. Results obtained by Fressengeas and Molinari (1994), Jeanclaude and Fressengeas (1997) are accurately retrieved in a straightforward way.

Acknowledgement

The authors thank Dr. Serge Cadet of LPMM/ University of Metz for fruitful discussions.

Appendix A. Analysis of the growth rate of perturbation for rate insensitive materials under axisymmetric loadings

A.1. The growth rate is a real number

Consider first the general case where the growth rate η is a complex number. Then the fourth order algebraic equation (27) can be written in the following form:

$$l^4 + (b_r + \mathrm{i}b_i)l^2 + c_r + \mathrm{i}c_i = 0 \tag{A.1}$$

where b_i and c_i are proportional to the imaginary part of η. In this case, four complex solutions can be found: l_1, $-l_1$, l_2 and $-l_2$. Note that when η is real, $l_1 = \overline{l}_2$.

Due to the axisymmetic conditions (24), Φ is searched in the form:

$$\Phi = R\sin(kZ)\{A_1 \mathrm{e}^{\eta t} I_1(l_1 R) + A_2 I_1 \mathrm{e}^{\eta t}(l_2 R)\} \tag{A.2}$$

where A_1 and A_2 are complex amplitude scalar.

The following notations are adopted:

$$C_1 = A_1 \mathrm{e}^{\eta t} \quad C_2 = A_2 \mathrm{e}^{\eta t} \tag{A.3}$$

and the Taylor expansion of the Bessel function I_1 is introduced:

$$I_1(R) = \sum_{k=0}^{+\infty} \frac{(R/2)^{1+2k}}{k!\Gamma(k+2)} \tag{A.4}$$

Moreover, the stream function Φ has to be real for any $0 \leqslant R \leqslant R_0$, thus the condition $\Phi = \overline{\Phi}$ implies, for any R:

$$\sum_{k=0}^{+\infty} \frac{C_1(l_1 R/2)^{1+2k} - \overline{C}_1(\overline{l}_1 R/2)^{1+2k} + C_2(l_2 R/2)^{1+2k} - \overline{C}_2(\overline{l}_2 R/2)^{1+2k}}{k!\Gamma(k+2)} = 0 \tag{A.5}$$

which leads to, for any k:

$$C_1(l_1)^{1+2k} - \overline{C}_1(\overline{l}_1)^{1+2k} + C_2(l_2)^{1+2k} - \overline{C}_2(\overline{l}_2)^{1+2k} = 0 \tag{A.6}$$

where $\overline{(\cdot)}$ designates the conjugate of the complex number $(\cdot)$. The only possible solution is

$$l_1 = \overline{l}_2 \tag{A.7}$$

which means that the fourth order algebraic equation (A.1) must have real coefficients. Therefore η is a real number.

A.2. Growth rates

It is shown in this section that the growth rate can only have two values. The growth rate η and the radial wavenumber l are solutions of the system formed by Eq. (27) and one of the following relationships (33), (35), (37) and (39). It is easily proved that these two relationships define even functions of l and quadratic functions of η. Therefore, the system can be written in the following form:

$$\eta^2 + B_1(l)\eta + C_1(l) = 0 \quad \eta^2 + B_2(l)\eta + C_2(l) = 0 \tag{A.8}$$

B_1, B_2, C_1 and C_2 are even functions of the parameter l. By combination, η can be viewed as an even function of l:

$$\eta = B_3(l) \tag{A.9}$$

As a conclusion, for each wavenumber k, the four complex radial wavenumbers l, solution of Eq. (27), can be merged into pairs of opposite complex numbers. Therefore, owing to Eq. (A.9), only two real growth rates are possible for the perturbation associated to the wavenumber k.

Appendix B. Initial conditions for the acceleration

For each longitudinal wavenumber k, two growth rates are found which provide two possible forms for the perturbation noted $\Phi^{(1)}$ and $\Phi^{(2)}$. Since a linear stability analysis is performed, any linear combination of the two modes satisfied the homogeneous boundary conditions and axisymmetry. For each k, the perturbation has the following form:

$$\Phi = [A_1 e^{\eta_1 t} f_1(R) + A_2 e^{\eta_2 t} f_2(R)] \sin kZ \tag{B.1}$$

where A_1 and A_2 are real constants.

It must be checked that at the time t_0^+, the perturbed acceleration derived from the stream function Φ is equal to zero. By time derivation of the relationship (19), the acceleration components are given by:

$$\gamma_r = -\frac{1}{2}\frac{V_0}{L_0}\epsilon'^{3/2}\frac{\Phi_{,Z}}{R} + \frac{\sqrt{\epsilon'}}{R}\dot{\Phi}_{,Z} \tag{B.2a}$$

$$\gamma_z = -\frac{V_0}{L_0}\frac{\Phi_{,R}}{R} - \frac{1}{R\epsilon'}\dot{\Phi}_{,R} \tag{B.2b}$$

It is easily seen that the two components of the acceleration vector are not equal to zero for any k. Nevertheless, for large values of k, it is clear that from Eq. (27) the 4 solutions l are almost not depending on η. As a consequence, the two functions $f_1(R)$ and $f_2(R)$ are identical. Thus by substitution of (B.1) into (B.2), it follows:

$$\gamma_r = k\left[A_1\left(\sqrt{\epsilon'}\eta_1 - \frac{1}{2}\frac{V_0}{L_0}\epsilon'^{3/2}\right) + A_2\left(\sqrt{\epsilon'}\eta_2 - \frac{1}{2}\frac{V_0}{L_0}\epsilon'^{3/2}\right)\right]\cos(kZ) f_1(R) \tag{B.3a}$$

$$\gamma_z = -\left[A_1\left(\frac{V_0}{L_0} + \frac{\eta_1}{\epsilon'}\right) + A_2\left(\frac{V_0}{L_0} + \frac{\eta_2}{\epsilon'}\right)\right]\sin(kZ) f_{1,R}(R) \tag{B.3b}$$

The two solutions η_1 and η_2 are the roots of the quadratic equation obtained from (27):

$$\rho\left(\epsilon' k^2 - \frac{l^2}{\epsilon'^2}\right)\eta^2 - \rho\frac{V_0}{L_0}\left(2\frac{l^2}{\epsilon'} + \epsilon'^2 k^2\right)\eta + \left(\mu - \frac{\sigma_e^0}{2}\right)\frac{l^4}{\epsilon'^3} + (\mu - 3\mu^*)k^2 l^2 + k^4\left(\mu + \frac{\sigma_e^0}{2}\right)\epsilon'^3 = 0 \tag{B.4}$$

From the boundary condition (23a) and from (25), the modulus of k is of the same order as the modulus of l. Thus from (B.4), the sum $\eta_1 + \eta_2$ is scaled by V_0/L_0 and the product $\eta_1\eta_2$ by the ratio $\sigma_e k^2/\rho$. As seen in Fig. 2, the maximum growth rate is positive and large compared to V_0/L_0. Then, the other possible growth rate (which is real) has to be negative, and of the same order of magnitude; then the other solution is also large compared to V_0/L_0. As a consequence, the relationships (B.3) can be simplified into:

$$\gamma_r = k\sqrt{\epsilon'}(A_1\eta_1 + A_2\eta_2)\cos(kZ) f_1(R) \tag{B.5a}$$

$$\gamma_z = -\frac{1}{\epsilon'}(A_1\eta_1 + A_2\eta_2)\sin(kZ) f_{1,R}(R) \tag{B.5b}$$

and the initial condition $\boldsymbol{\gamma} = \mathbf{0}$ is fulfilled when

$$A_1\eta_1 + A_2\eta_2 = 0 \tag{B.6}$$

In our analysis, when the amplitude factors A_1 and A_2 are linked by Eq. (B.6), an initial velocity perturbation (of the form (B.1)) can be added to the background solution with no initial acceleration. It has been checked from the numerical simulations, that this condition is valid for longitudinal modes in the range where the growth rate is maximum, which is the case of interest in our analysis.

References

Altynova, M., Hu, X., Daehn, G.S., 1996. Increased ductility in high velocity electromagnetic ring expansion. Metallurgical and Materials Transactions 27A, 1837–1844.

Benallal, A., Tvergaard, V., 1995. Nonlocal continuum effects on bifurcation in the plane strain tension-compression test. Journal of the Mechanics and Physics of Solids 43, 741–770.

Chou, P.C., Carleone, J., Tanzio, C.A., Ciccarelli, R.D., 1977. Shaped charge jet breakup measurements and surface instability calculations. Tech. Rep. BRL-CR-337.

Considère, A., 1885. Ann. Ponts Chaussées 9, 574–575.

Fressengeas, C., Molinari, A., 1985. Inertia and thermal effects on the localization of plastic flow. Acta Metallurgica 33, 387–396.

Fressengeas, C., Molinari, A., 1994. Fragmentation of rapidly stretching sheets. European Journal of Mechanics A/Solids 13, 251–268.

Grady, D.E., Benson, D.A., 1983. Fragmentation of metal rings by electromagnetic loading. Experimental Mechanics 12, 393–400.

Han, J., Tvergaard, V., 1995. Effect of inertia on the necking as a precursor to dynamic fracture. European Journal of Mechanics A/Solids 14, 287–307.

Hill, R., Hutchinson, J.W., 1975. Bifurcation phenomena in the plane tension test. Journal of the Mechanics and Physics of Solids 23, 239–264.

Hollomon, J.H., 1945. Tensile deformation. Transactions of the American Institute of Mining and Metallurgical Engineers 162, 268–290.

Hutchinson, J.W., Neale, K., 1977. Influence of strain rate sensitivity on necking under uniaxial tension. Acta Metallurgica 25, 839–846.

Hutchinson, J.W., Neale, K., Needleman, A., 1978. Sheet necking I—validity of plane stress assumptions on the long wavelength approximation. In: Koistinen, D.P., Wang, N.M. (Eds.), Mechanics of Sheet Metal Forming. Plenum, NY, pp. 111–126.

Jeanclaude, V., Fressengeas, C., 1997. Dynamic necking of rods at high strain rates. Journal de Physique IV Colloque C3 7, 699–704.

Karpp, R.R., Simon, J., 1976. An estimate of the strength of a copper shaped charge jet and the effect of strength on the breakup of a stretching jet. Tech. Rep. BRL-1983.

Malvern, L.E., 1969. Introduction to the Mechanics of a Continuous Medium. Prentice-Hall, New Jersey.

Niordson, F.I., 1965. A unit for testing materials at high strain rates. Experimental Mechanics 5, 29–32.

Ozisik, M.N., 1968. Boundary Values Problems of Heat Conduction. Dover, New York.

Shenoy, V.B., Freund, L.B., 1999. Necking bifurcations during high strain rate extension. Journal of the Mechanics and Physics of Solids 47, 2209–2233.

Sorensen, N.J., Freund, L.B., 1998. Dynamic bifurcation during high-rate planar extension of a thin rectangular block. European Journal of Mechanics A/Solids 17, 709–724.

Storen, S., Rice, J.R., 1975. Localized necking in thin sheets. Journal of the Mechanics and Physics of Solids 23, 421–441.

Young, N.J.B., 1976. Bifurcation phenomena in the plane strain compression test. Journal of the Mechanics and Physics of Solids 24, 77–91.